ELSEVIER

Journal of Fluids and Structures 19 (2004) 1117–1128

JOURNAL OF FLUIDS AND STRUCTURES

www.elsevier.nl/locate/jnlabr/yjfls

Effect of decoupled fluid loading on nonlinear vibration of a flat plate

A. Tosh, A. Frendi*

Department of Mechanical and Aerospace Engineering, University of Alabama in Huntsville, 5000 Technology Drive, Tech Hall N264, Huntsville, AL 35899, USA

Received 7 January 2004; accepted 25 July 2004

Abstract

Numerical simulations of nonlinear responses of a flat plate subject to decoupled fluid loading are carried out. Under clamped boundary conditions and subject to forced vibration at its natural frequency corresponding to the (5,1) mode, the various response modes of the plate are determined. It is found that increasing the excitation amplitude, the response changed from periodic to chaotic. In addition, the fluid-wall shear stresses are found to change the response from linear to nonlinear and vice versa depending on their magnitudes. When a static pressure load is combined with fluid-wall shear stresses and low excitation amplitude, the resulting response was chaotic.

1. Introduction

It is known in structural dynamics that linear theory offers poor response predictions at high sound pressure levels, as observed experimentally by Bennouna and White (1984). Consequently, several nonlinear models have been proposed to overcome this weakness of linear theory. Mei and Prasad (1987) used a nonlinear damping model to explain some phenomena observed in the response of aircraft panels at high excitation levels. Reinhall and Miles (1989) studied the effect of damping and stiffness on random vibration of periodic plates, showing that response spectra could broaden due to the existence of nonlinear stiffness without introducing nonlinear damping. Robinson and Mei (1989) showed that nonlinear damping is actually responsible for the narrowing of the spectrum. A model based on geometric nonlinearity was used by Maestrello and Frendi (1992) and shown to overestimate the broadening of the response spectrum. In all the above studies, the fluid–structure coupling was neglected. Recently, Frendi et al. (1994) showed the existence of strong coupling between plate vibration and the surrounding flow field. Applying random excitations to the structure and using a fully coupled model, Frendi and Robinson (1993) were able to explain some of the results observed experimentally (Robinson et al., 1992). The studies of Frendi et al. (1994) also showed a change from linear to nonlinear response due to the amplitude of excitation. Frendi (1997a) obtained similar results using a two-dimensional-coupled model. Using a fully coupled model, computational studies on noise transmission from a turbulent boundary layer evolving over a flexible structure have been performed by Frendi (1997b). The results agreed well with those of the wind tunnel studies performed by Maestrello (1969) and thus revealed the importance of the coupled model. More recently, Frendi (2001) then Buhler and Frendi (2004) showed the importance of accounting for the fluid-wall shear

*Corresponding author.
E-mail address: frendi@eng.uah.edu (A. Frendi).

0889-9746/$ - see front matter © 2004 Elsevier Ltd. All rights reserved.
doi:10.1016/j.jfluidstructs.2004.07.003

stresses on the nonlinear structural response. It was found that under certain conditions, fluid-wall shear stresses reduced the level of structural vibration and changed the response from nonlinear to linear.

The objective of the current research is to extend the previous one-dimensional studies to a two-dimensional, clamped flat plate. In particular, an in-depth study of its nonlinear response under decoupled fluid loading will be carried-out. The effects of pressure fluctuation amplitude (source of structural vibration), fluid-wall shear stresses, static pressure and combinations of these forces on the structural response of a plate will be studied.

2. Mathematical model

Starting from Cauchy's first law of motion (Chung, 1996), one can obtain the equations of motion of a plate in Cartesian coordinates

$$\left(\frac{\partial^2 M_{xx}}{\partial x^2}+2\frac{\partial^2 M_{xy}}{\partial x\partial y}+\frac{\partial^2 M_{yy}}{\partial y^2}\right)+\left(N_{xx}\frac{\partial^2\eta}{\partial x^2}+2N_{xy}\frac{\partial^2\eta}{\partial x\partial y}+N_{yy}\frac{\partial^2\eta}{\partial y^2}\right)+\frac{\partial}{\partial x}\left[\sigma_{zx}(\eta+h/2)\right]+\frac{\partial}{\partial y}\left[\sigma_{zy}(\eta+h/2)\right]+[\sigma_{zz}]_{-h/2}^{+h/2}=\rho h\frac{\partial^2\eta}{\partial t^2}, \tag{1}$$

where

$$M_{xx}=\int_{-h/2}^{h/2}\sigma_{xx}z\,\mathrm{d}z,\quad M_{yy}=\int_{-h/2}^{h/2}\sigma_{yy}z\,\mathrm{d}z,\quad M_{xy}=\int_{-h/2}^{h/2}\sigma_{yx}z\,\mathrm{d}z, \tag{2}$$

$$N_{xx}=\int_{-h/2}^{h/2}\sigma_{xx}\,\mathrm{d}z,\quad N_{yy}=\int_{-h/2}^{h/2}\sigma_{yy}\,\mathrm{d}z,\quad N_{xy}=\int_{-h/2}^{h/2}\sigma_{yx}\,\mathrm{d}z, \tag{3}$$

with σ_{ij} being the stresses, ρ the density of the plate material, h the plate thickness and η the transverse displacement. Assuming fluid flow on one side of the plate only, the stresses along the zx, zy and zz directions are the fluid-wall shear stresses for the first two and normal pressure across the plate for the last.

Applying stress–strain relations, one can evaluate the integrals of Eqs. (2) and (3) and express the second-order derivatives of the moments in terms of η in Eq. (1). Stress–strain relations of linear form are intuitively applicable to Eqs. (2), since these terms will finally correspond to the linear components of the plate equation. Nonlinear integrated stress–strain relations, those needed to be used in Eq. (3), can be derived using St. Venant's principle with the assumptions of plate theory (Vinson, 1974). The general formulations of stress–strain relations are

$$\sigma_{xx}=\frac{E}{(1-v^2)}(\gamma_{xx}+v\gamma_{yy}),\quad \sigma_{yy}=\frac{E}{(1-v^2)}(v\gamma_{xx}+\gamma_{yy}),\quad \sigma_{yx}=\frac{E}{(1+v)}\gamma_{yx}, \tag{4}$$

where the γ terms represent the strain tensor.

St. Venant's principle is given as

$$u(x,y,z)=u_0(x,y)+z\alpha(x,y), \tag{5}$$

$$v(x,y,z)=v_0(x,y)+z\beta(x,y), \tag{6}$$

$$w=\eta(x,y), \tag{7}$$

where, u_0 and v_0 represent in-plane displacements along the x- and y-directions, and u, v and w are displacements along the x-, y-, and z-directions. Using the nonlinear strain relations in Cartesian coordinates (Chung, 1996) and from the plate theory assumption $\gamma_{xz}=\gamma_{yz}=0$, the unknown terms α and β can be obtained as

$$\alpha=-\frac{\partial\eta}{\partial x}\quad\text{and}\quad\beta=-\frac{\partial\eta}{\partial y}. \tag{8}$$

Thus, using the displacement Eqs. (5)–(7), in the general stress–strain relations in Eq. (4), the nonlinear terms in Eq. (3) can be obtained as

$$N_{xx}=\frac{E}{(1-v^2)}\left[\frac{h}{2}\left(\frac{\partial\eta}{\partial x}\right)^2+v\frac{h}{2}\left(\frac{\partial\eta}{\partial y}\right)^2\right], \tag{9}$$

$$N_{yy} = \frac{E}{(1-v^2)}\left[v\frac{h}{2}\left(\frac{\partial\eta}{\partial x}\right)^2 + \frac{h}{2}\left(\frac{\partial\eta}{\partial y}\right)^2\right], \tag{10}$$

$$N_{xy} = \frac{E}{(1+v)}\left[\frac{h}{2}\left(\frac{\partial\eta}{\partial x}\frac{\partial\eta}{\partial y}\right)\right]. \tag{11}$$

Higher-order derivatives of η, both with respect to x and y are neglected while obtaining the equations above. To represent the nonlinear stiffness of the plate, the above terms are integrated over the plate surface and normalized by the plate area L_xL_y.

The plate equation in terms of the transverse displacement (η) can then be expressed as

$$\begin{aligned} &D\left(\frac{\partial^4\eta}{\partial x^4} + 2\frac{\partial^4\eta}{\partial x^2\partial y^2} + \frac{\partial^4\eta}{\partial y^4}\right) - \left(\overline{N_{xx}}\frac{\partial^2\eta}{\partial x^2} + 2\overline{N_{xy}}\frac{\partial^2\eta}{\partial x\partial y} + \overline{N_{yy}}\frac{\partial^2\eta}{\partial y^2}\right) \\ &\quad - \left[\tau_{zx}\frac{\partial\eta}{\partial x} + \tau_{zy}\frac{\partial\eta}{\partial y} + \eta\left(\frac{\partial\tau_{zx}}{\partial x} + \frac{\partial\tau_{zy}}{\partial y}\right)\right] + \rho h\frac{\partial^2\eta}{\partial t^2} + \Gamma\frac{\partial\eta}{\partial t} \\ &= \Delta p(t) + \frac{h}{2}\left(\frac{\partial\tau_{zx}}{\partial x} + \frac{\partial\tau_{zy}}{\partial y}\right) + \Delta p_{\text{static}}, \end{aligned} \tag{12}$$

where $D = Eh^3/[12(1-v^2)]$ is the bending stiffness with E being Young's modulus and v Poisson's ratio; τ_{zx}, τ_{zy} are the fluid wall shear stresses, Γ the physical damping, $\Delta p(t)$ the pressure differential across the plate and Δp_{static} the static pressure. The nonlinear stiffness terms $(\overline{N_{xx}}, \overline{N_{yy}}, \overline{N_{xy}})$ representing average tensions over the plate surface are written as

$$\overline{N_{xx}} = \frac{Eh}{2(1-v^2)L_xL_y}\left[\int_0^{L_x}\int_0^{L_y}\left(\frac{\partial\eta}{\partial x}\right)^2 \mathrm{d}x\,\mathrm{d}y + v\int_0^{L_x}\int_0^{L_y}\left(\frac{\partial\eta}{\partial y}\right)^2 \mathrm{d}x\,\mathrm{d}y\right], \tag{13}$$

$$\overline{N_{yy}} = \frac{Eh}{2(1-v^2)L_xL_y}\left[v\int_0^{L_x}\int_0^{L_y}\left(\frac{\partial\eta}{\partial x}\right)^2 \mathrm{d}x\,\mathrm{d}y + \int_0^{L_x}\int_0^{L_y}\left(\frac{\partial\eta}{\partial y}\right)^2 \mathrm{d}x\,\mathrm{d}y\right], \tag{14}$$

$$\overline{N_{xy}} = \frac{Eh}{2(1+v)L_xL_y}\left[\int_0^{L_x}\int_0^{L_y}\left(\frac{\partial\eta}{\partial x}\right)\left(\frac{\partial\eta}{\partial y}\right) \mathrm{d}x\,\mathrm{d}y\right], \tag{15}$$

where, L_x and L_y are the plate lengths along the x- and y-directions, respectively.

The clamped boundary conditions on all sides of the plate can be expressed in terms of η as

$$\eta\big|_{x=0} = 0 \quad \eta\big|_{x=L_x} = 0 \quad \eta\big|_{y=0} = 0 \quad \eta\big|_{y=L_y} = 0, \tag{16}$$

$$\left.\frac{\partial\eta}{\partial x}\right|_{x=0} = 0 \quad \left.\frac{\partial\eta}{\partial x}\right|_{x=L_x} = 0 \quad \left.\frac{\partial\eta}{\partial y}\right|_{y=0} = 0 \quad \left.\frac{\partial\eta}{\partial y}\right|_{y=L_y} = 0. \tag{17}$$

3. Results and discussions

The material properties used for the plate were those of aluminum with Young's modulus, $E = 74.14\,\text{GPa}$, Poisson's ratio, $v = 0.30$, density, $\rho = 2700\,\text{kg/m}^3$, plate length, $L_x = 0.305\,\text{m}$, plate width, $L_y = 0.203\,\text{m}$ and plate thickness, $h = 1.016 \times 10^{-3}$ m. The natural frequencies of the plate were determined and found to be 165.7, 255.6, 399.9, 405.7, 483.4, 610.1, 624.2, 743.2, 820.3, 824.5, 863.9, 960.7 Hz for the first few modes. A frequency corresponding to the symmetric (5,1) mode ($f = 863.9\,\text{Hz}$) was chosen as the excitation frequency.

The plate equation was discretized spatially by second-order central differencing. An implicit temporal scheme obtained by Hoff and Pahl (1988a,b) was used. All simulations were performed with a physical damping of $\Gamma = 152.01\,\text{N s/m}^3$.

The following results are obtained from the various studies on plate response under the individual and combined effects of excitation amplitude, fluid-wall shear stresses and static pressure. The pressure differential across the plate used is a function of the form $\Delta p(t) = \varepsilon\sin(\omega t)$, with ε the nondimensional excitation amplitude (reference

$1.01 \times 10^5\ \mathrm{N/m^2}$) and $\omega = 2\pi f$ the frequency of excitation. In what follows, only responses at the center of the plate are given with plots of time history, phase diagram and power spectra.

3.1. Effect of excitation amplitude

In the absence of fluid-wall shear stresses and static pressure, increasing the excitation amplitude, ε, within the range 0.075–0.27, changes the response from linear to quasi-linear then to highly nonlinear. The power spectrum, Fig. 1(c), shows that for $\varepsilon = 0.075$ the response is linear with a dominant fundamental frequency ($f = 863.9$ Hz). This is confirmed by a harmonic time history, Fig. 1(a), and a circular phase diagram, Fig. 1(b). In Fig. 2, the response changes to a quasi-linear mode with a higher level of the high harmonic, *3f*, as the excitation is increased to $\varepsilon = 0.20$, Fig. 2(c). The phase diagram is noncircular, Fig. 2(b), but the time history still shows one dominant frequency, Fig. 2(a).

At $\varepsilon = 0.25$, the response changes to nonlinear with the appearance of the sub-harmonic, *f/3*, along with its harmonics, Fig. 3(c). Three loops are shown on the phase diagram, Fig. 3(b) and the time history now shows the presence of at least one additional frequency, Fig. 3(a). At $\varepsilon = 0.27$ the response is highly nonlinear with a strong *f/3* along with its harmonics, Fig. 4(c). Two quasi-periodic loops appear in the phase diagram, Fig. 4(b), and the time history shows the presence of several frequencies, Fig. 4(a). Further increasing the amplitude beyond 0.27, the response returns to a quasi-linear mode similar to that shown on Fig. 2.

3.2. Effect of fluid-wall shear stresses

The following studies have been carried out for the linear and nonlinear excitation amplitude cases studied above. Fluid-wall shear stresses are now added to the excitation. The first case involves a study on the effect of fluid-wall shear stresses together with an excitation of amplitude of $\varepsilon = 0.20$, for which the response was originally linear. The second case involves the same effect with an excitation amplitude of $\varepsilon = 0.25$ for which the response was nonlinear. The flow direction depends on the magnitudes of τ_{zx} and τ_{zy} used. The cross-direction is arbitrarily set to 10% of the other.

Under an excitation amplitude of $\varepsilon = 0.2$ and a nondimensional wall shear stress (reference $1.01 \times 10^5\ \mathrm{N/m^2}$) in the x-direction of $\tau_{zx} = 1.0$, the response is unchanged from that without the wall shear stress, compare Figs. 5–2. Increasing τ_{zx} to 1.5, the response changes to nonlinear, with a three loops phase diagram, Fig. 6(b), a time history with at least two frequencies, Fig. 6(a), and a power spectrum showing a strong sub-harmonic *f/3*, Fig. 6(c).

Further increasing the wall shear stress τ_{zx} to 1.75, the response returns to a quasi-linear mode of vibration, Fig. 7. The power spectrum shows several peaks surrounding both the harmonic, *3f*, and the fundamental, *f*, Fig. 7(c). Similarly, the phase diagram shows one quasi-periodic loop, Fig. 7(b).

For an excitation amplitude ε of 0.25 and a wall shear stress τ_{zx} of 1.0, the response is again unchanged (i.e., nonlinear), compare Figs. 8–3. Increasing τ_{zx} to 1.5, the response changes to a quasi-linear mode, Fig. 9. The phase diagram changes back to a single, quasi-periodic, noncircular loop, Fig. 9(b), with a harmonic time history, Fig. 9(a). Further increasing τ_{zx} to 1.75 the response becomes highly nonlinear, Fig. 10, with dominant *f* and 5*f*/3 along with the subharmonic, *f*/3, Fig. 10(c). The phase diagram shows nonrepetitive loops, Fig. 10(b), and the time history shows the presence of several frequencies, Fig. 10(a).

When the fluid flow is considered along the y-direction, τ_{zx} is made to be 10% of τ_{zy}, the response does not change much from the original (without fluid-wall stresses). Also, assuming a diagonal flow over the plate surface (with $\tau_{zx} = \tau_{zy}$), the response changes from linear to nonlinear and vice versa at the same amplitudes as those obtained with flow along x-direction. These results indicate that the nature of the response for the (5,1) mode is affected only when the fluid flow is along the x-direction.

3.3. Effect of static pressure

Adding a static pressure as an external force on the plate surface, similar simulations were carried out with variations of excitation amplitude and fluid-wall shear stresses. At a constant nondimensional static pressure of $\Delta p_{\mathrm{static}} = 0.5$ (reference $1.01 \times 10^5\ \mathrm{N/m^2}$), $\varepsilon = 0.20$ and with negligible fluid-wall shear stresses, the response is quasi-linear. The power spectrum, Fig. 11(c), reveals contributions of several harmonics. As the fluid-wall shear stresses are applied and gradually increased to $\tau_{zx} = 1.5$, the response becomes chaotic, Fig. 12. There is no apparent periodicity in the time history, Fig. 12(a), and the phase diagram shows several loops, Fig. 12(b). The power spectrum shows several subharmonics and harmonics of nearly equal strength to the fundamental, Fig. 12(c).

For $\varepsilon = 0.25$, similar trends of response are obtained (Figs. 13 and 14). When no wall shear stresses are applied the response is quasi-linear, Fig. 13. However, when $\tau_{zx} = 1.5$ is applied the plate response is nonlinear. One should notice that the time history, Fig. 14(a), and the phase diagram, Fig. 14(b), show a weakly nonlinear behavior. The power

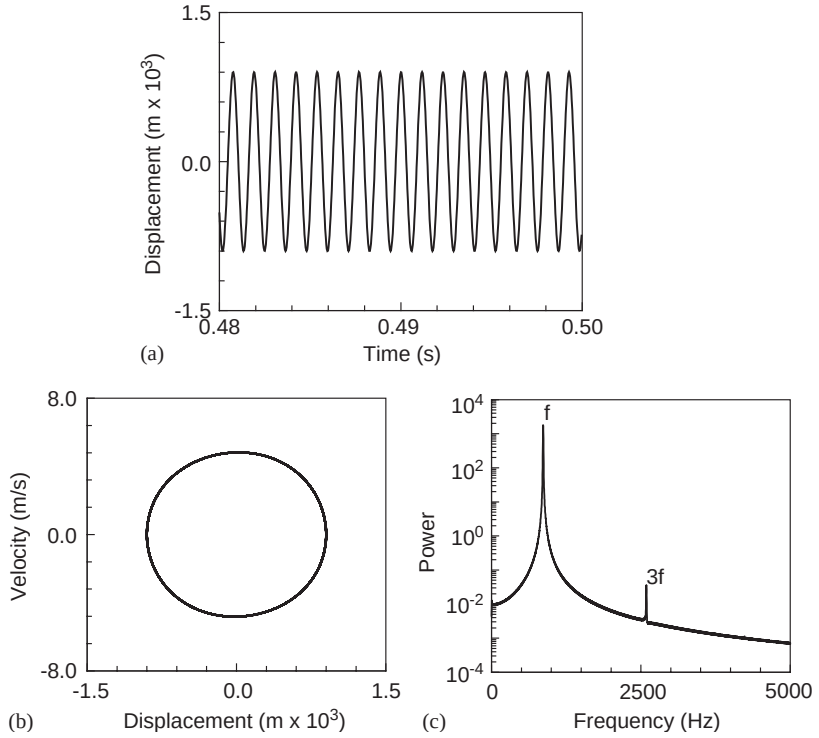

Fig. 1. Linear plate response for $\varepsilon = 0.075$; $\tau_{zx} = 0.0$, $\tau_{zy} = 0.0$; $\Delta p_{static} = 0.0$:(a) time history, (b) phase diagram, and (c) power spectrum.

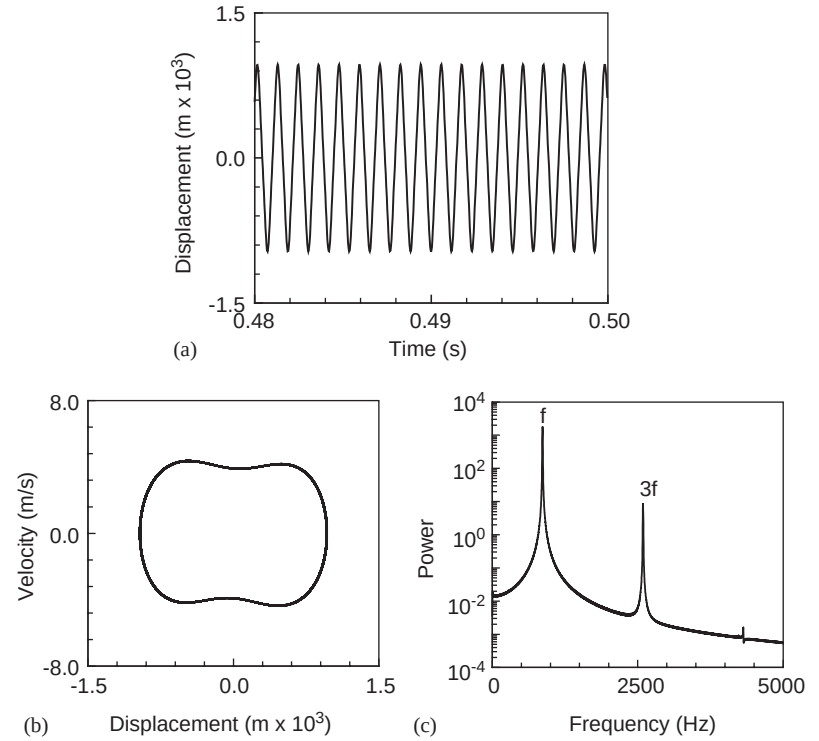

Fig. 2. Quasi-linear plate response for $\varepsilon = 0.20$; $\tau_{zx} = 0.0$, $\tau_{zy} = 0.0$; $\Delta p_{static} = 0.0$: (a) time history, (b) phase diagram, and (c) power spectrum.

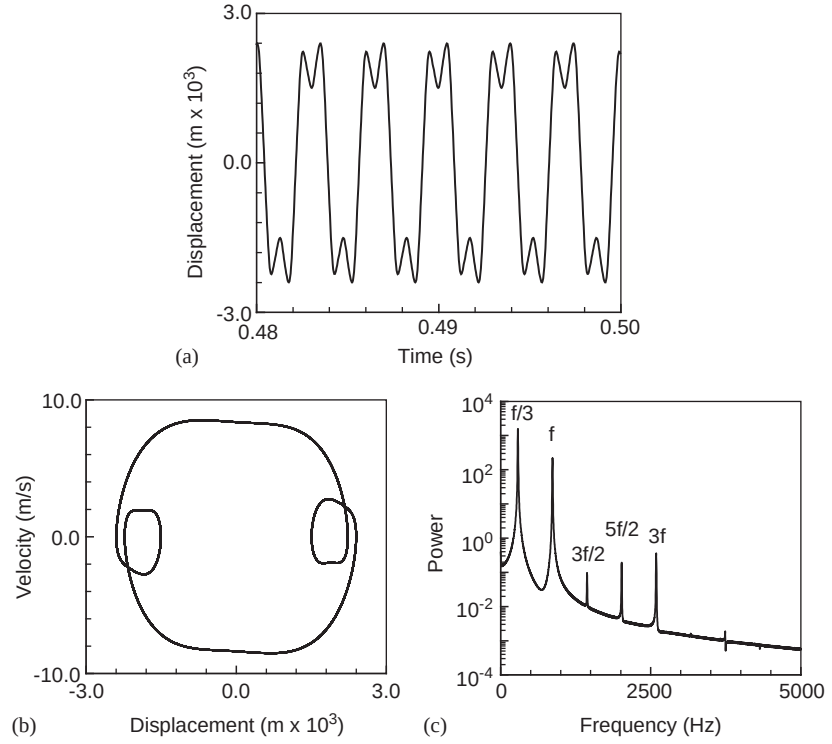

Fig. 3. Nonlinear plate response for $\varepsilon = 0.25$; $\tau_{zx} = 0.0$, $\tau_{zy} = 0.0$; $\Delta p_{static} = 0.0$: (a) time history, (b) phase diagram, and (c) power spectrum.

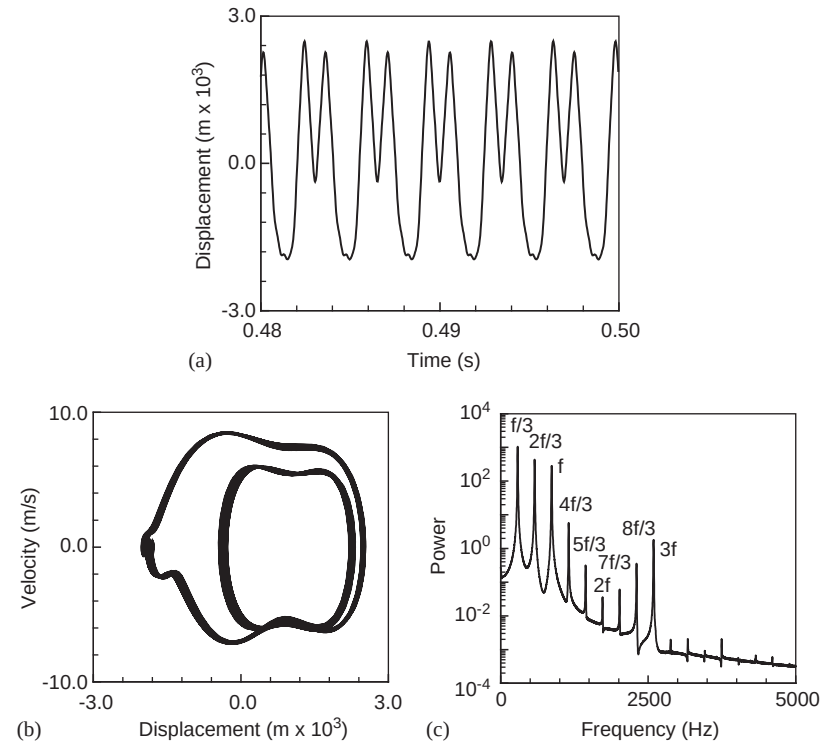

Fig. 4. Highly nonlinear plate response for $\varepsilon = 0.27$; $\tau_{zx} = 0.0$, $\tau_{zy} = 0.0$; $\Delta p_{static} = 0.0$: (a) time history, (b) phase diagram, and (c) power spectrum.

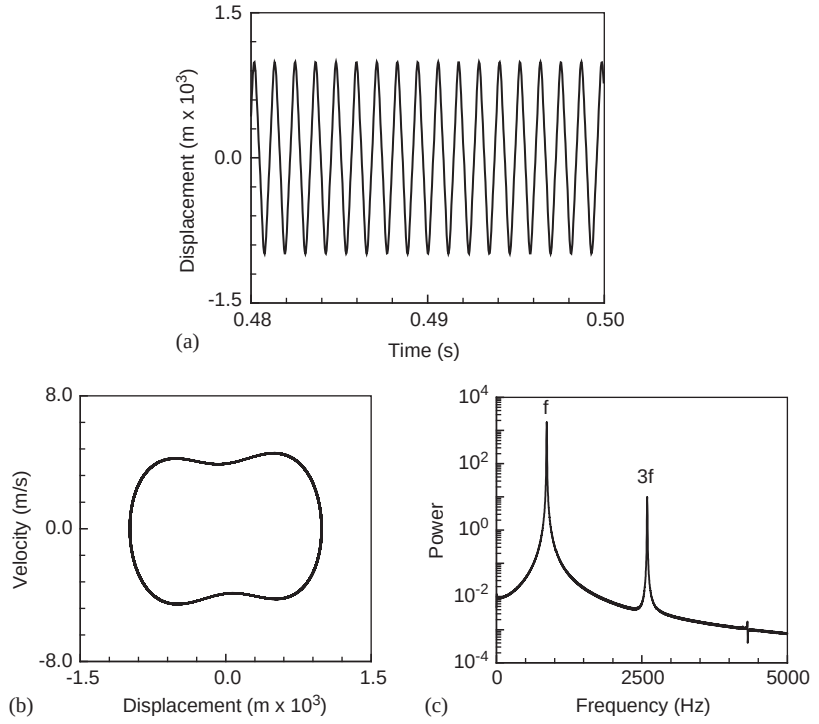

Fig. 5. Quasi-linear plate response for $\varepsilon = 0.20$; $\tau_{zx} = 1.0$, $\tau_{zy} = 0.10$; $\Delta p_{static} = 0.0$: (a) time history, (b) phase diagram, and (c) power spectrum.

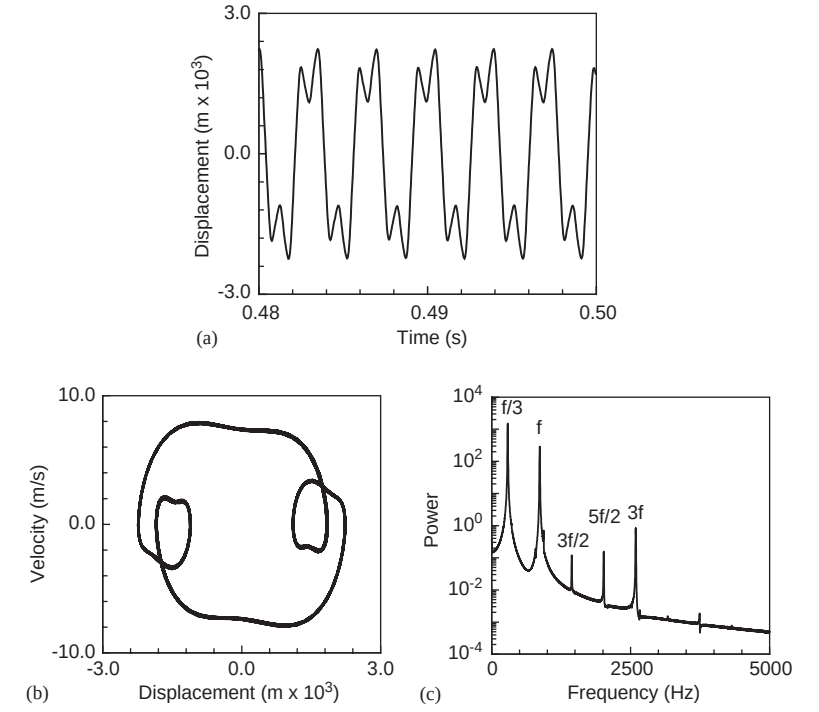

Fig. 6. Nonlinear plate response for $\varepsilon = 0.20$; $\tau_{zx} = 1.5$, $\tau_{zy} = 0.15$; $\Delta p_{static} = 0.0$: (a) time history, (b) phase diagram, and (c) power spectrum.

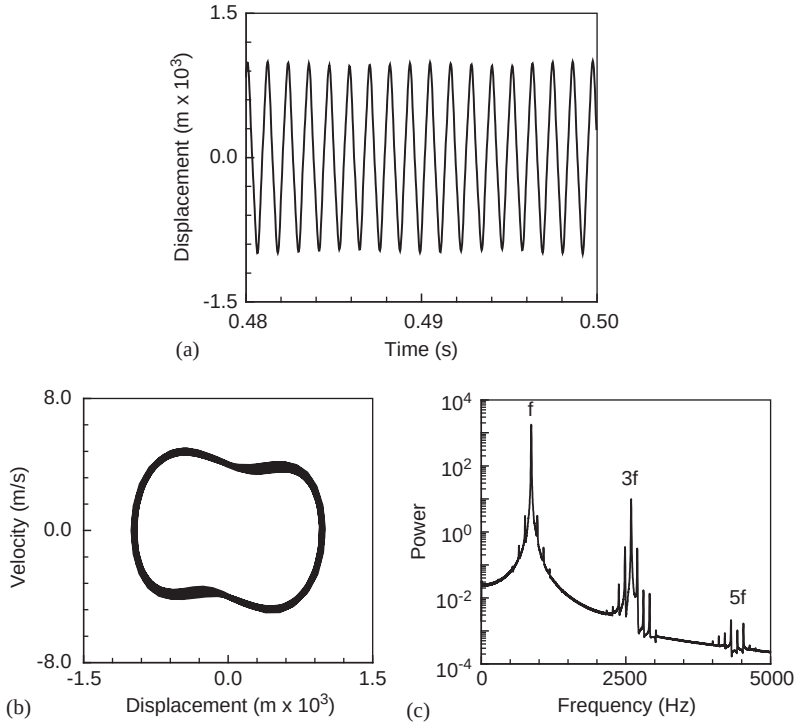

Fig. 7. Quasi-linear plate response for $\varepsilon = 0.20$; $\tau_{zx} = 1.75$, $\tau_{zy} = 0.175$; $\Delta p_{\text{static}} = 0.0$: (a) time history, (b) phase diagram, and (c) power spectrum.

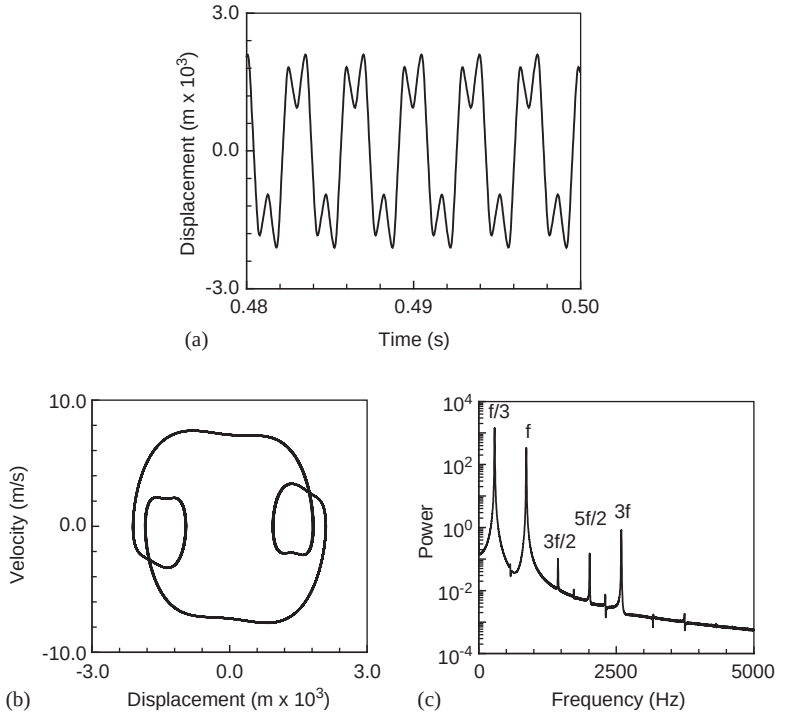

Fig. 8. Nonlinear plate response for $\varepsilon = 0.25$; $\tau_{zx} = 1.0$, $\tau_{zy} = 0.10$; $\Delta p_{static} = 0.0$: (a) time history, (b) phase diagram, and (c) power spectrum.

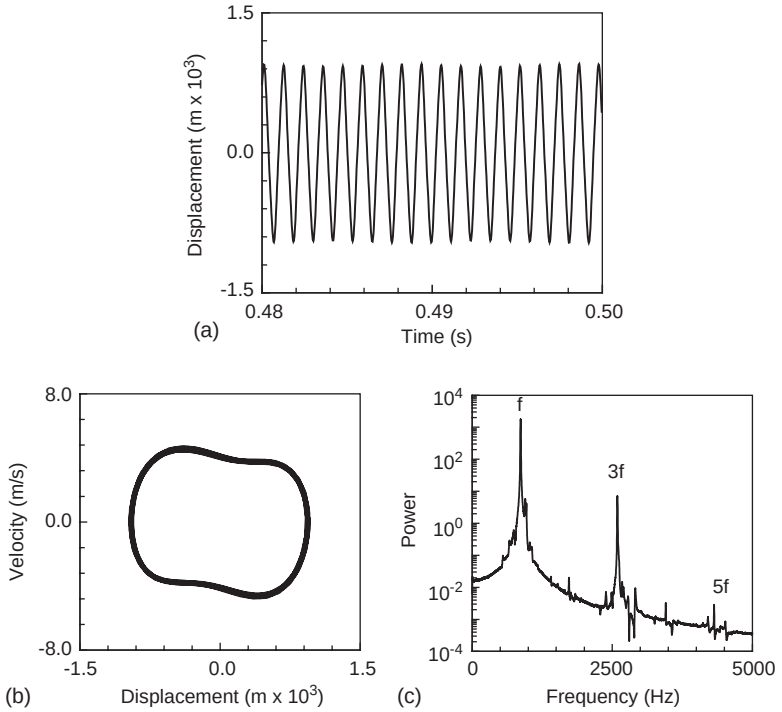

Fig. 9. Quasi-linear plate response for $\varepsilon = 0.25$; $\tau_{zx} = 1.5$, $\tau zy = 0.15$; $\Delta p_{static} = 0.0$: (a) time history, (b) phase diagram, and (c) power spectrum.

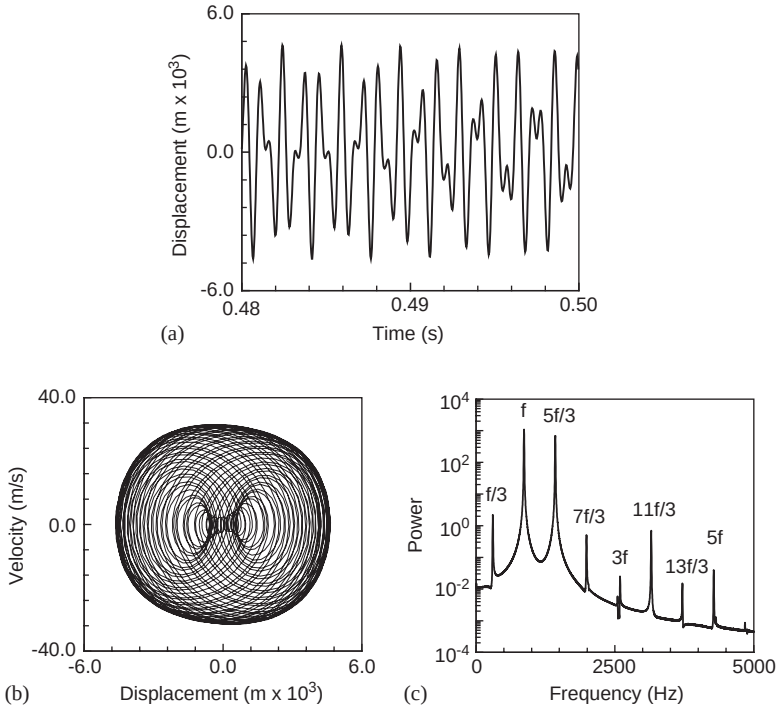

Fig. 10. Highly nonlinear plate response for $\varepsilon = 0.25$; $\tau_{zx} = 1.75$, $\tau_{zy} = 0.175$; $\Delta p_{static} = 0.0$: (a) time history, (b) phase diagram, and (c) power spectrum.

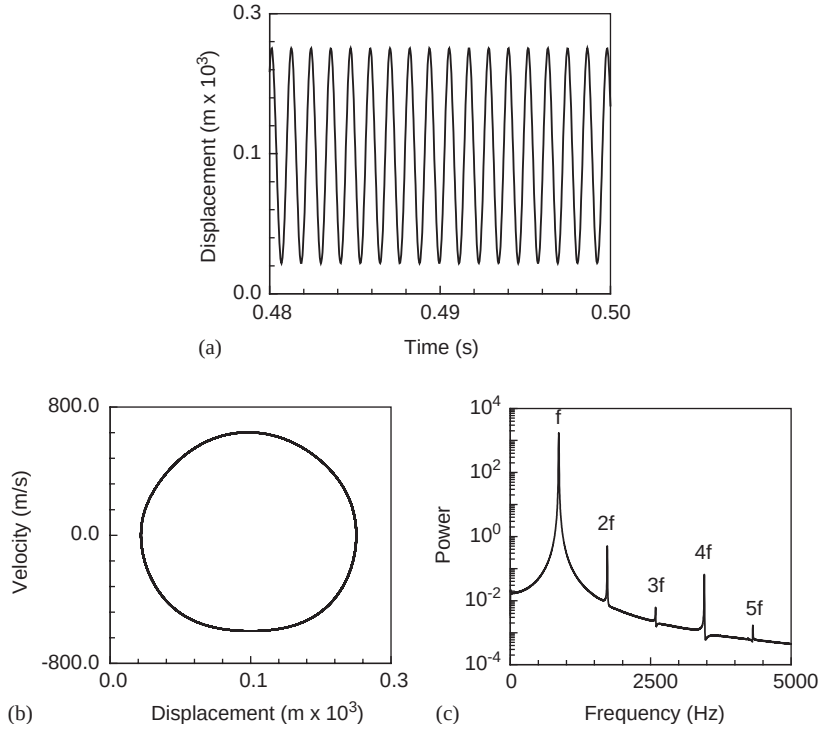

Fig. 11. Quasi-linear plate response for $\varepsilon = 0.20$; $\tau_{zx} = 0.0$, $\tau_{zy} = 0.0$; $\Delta p_{static} = 0.5$: (a) time history, (b) phase diagram, and (c) power spectrum.

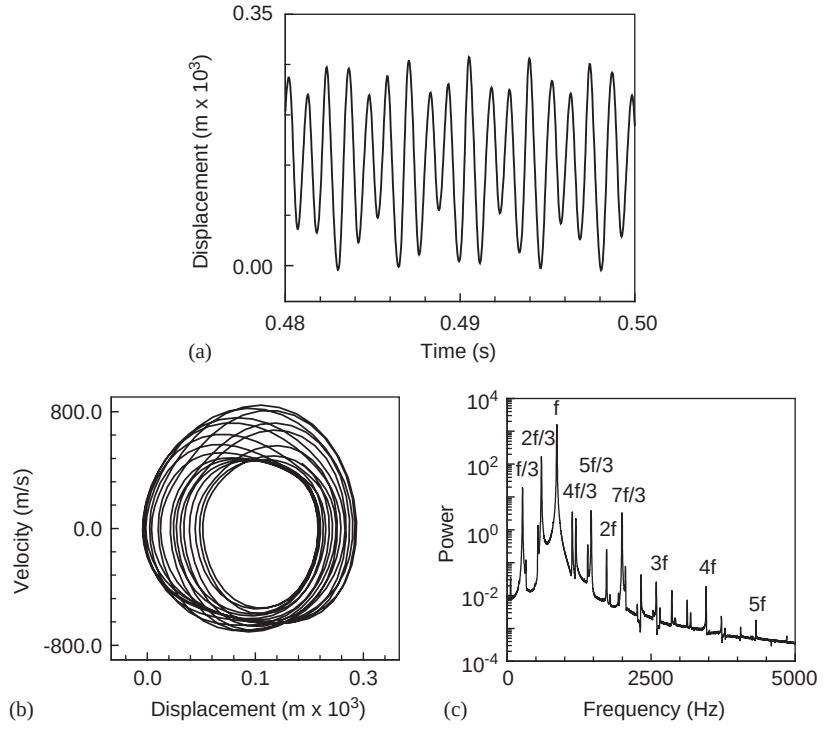

Fig. 12. Chaotic plate response for $\varepsilon = 0.20$; $\tau_{zx} = 1.5$, $\tau_{zy} = 0.15$; $\Delta p_{static} = 0.5$: (a) time history, (b) phase diagram, and (c) power spectrum.

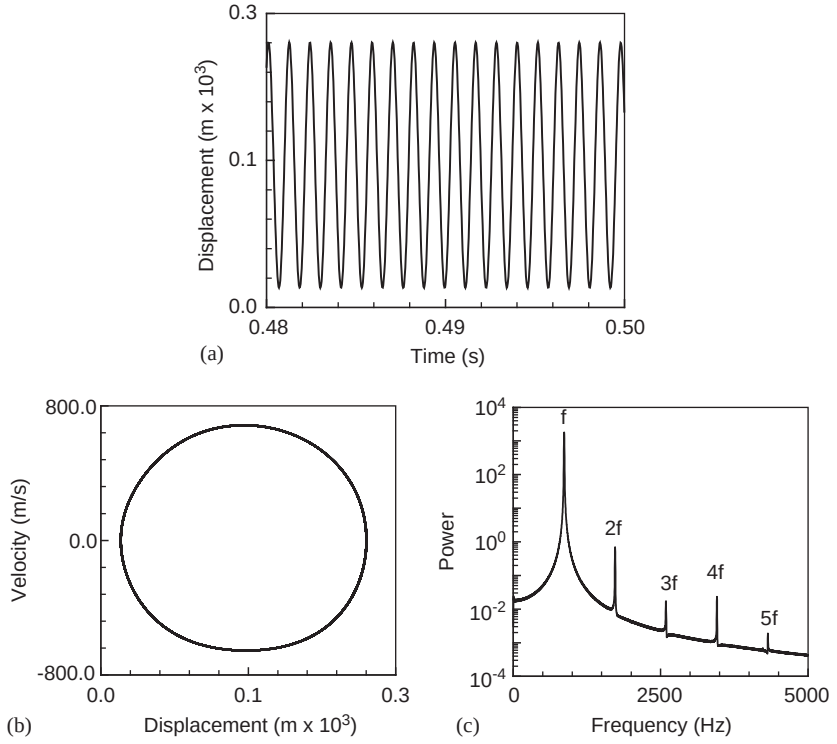

Fig. 13. Quasi-linear plate response for $\varepsilon = 0.25$; $\tau_{zx} = 0.0$, $\tau_{zy} = 0.0$; $\Delta p_{static} = 0.5$: (a) time history, (b) phase diagram, and (c) power spectrum.

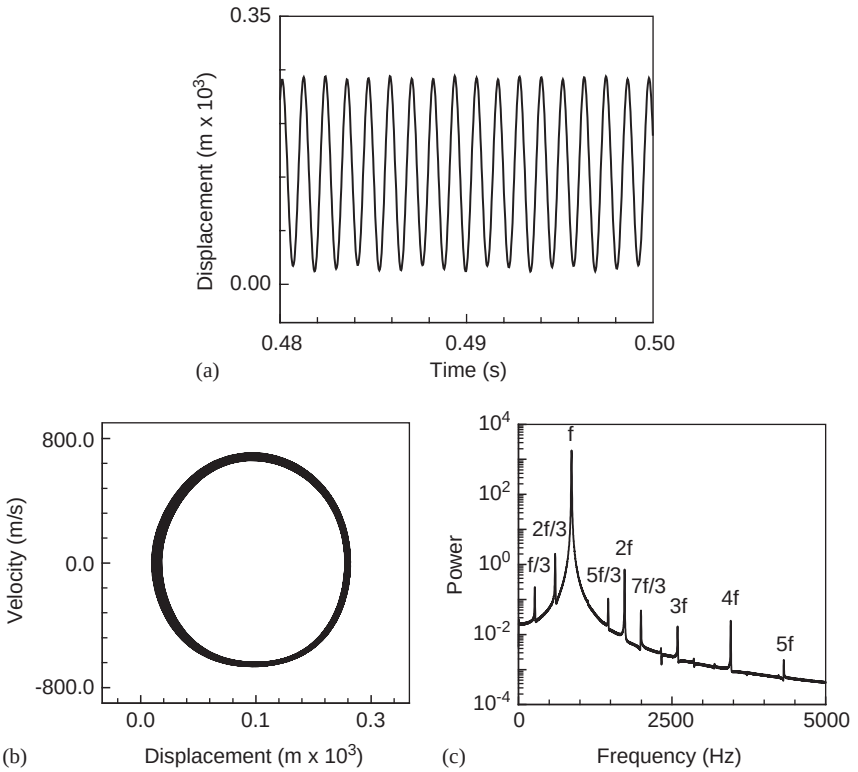

Fig. 14. Nonlinear plate response for $\varepsilon = 0.25$; $\tau_{zx} = 1.5$, $\tau_{zy} = 0.15$; $\Delta p_{static} = 0.5$: (a) time history, (b) phase diagram, and (c) power spectrum.

spectrum, Fig. 14(c), shows the presence of weak subharmonics and harmonics. This behavior is attributed to the presence of curvature on the plate due to the static pressure load. The natural frequencies under this static pressure were recalculated and found to be 624.6, 753.2, 987.1, 1127.5, 1221.1, 1338.0, 1431.6, 1536.8, 1724.0, 1817.5, 2004.7, 2180.1 Hz for the first few modes.

4. Concluding remarks

Studies on the effect of excitation amplitude show that by increasing the magnitude of pressure differential across the plate, the response changes from quasi-linear to a highly nonlinear behavior. The transition from linear to nonlinear appears to follow the following sequences: (i) dominant fundamental (linear), (ii) fundamental with harmonics (quasi-linear) and (iii) fundamental with subharmonics and harmonics (nonlinear). Application of fluid-wall shear stresses with increasing magnitudes effectively changes the response sequence (i.e., from linear-to-nonlinear or vice versa), depending on the initial response corresponding to the excitation amplitude. The presence of static pressure causes bending of the plate and hence reduces the level on nonlinearity of the response.

Acknowledgements

Financial support for this work was provided by a grant from the Office of Naval Research (ONR, Grant No. N00014-01-1-0128, technical monitor Dr Luise Couchman).

References

Bennouna, M., White, R.G., 1984. The effect of large vibration amplitudes on the dynamic strain response of a clamped–clamped beam with consideration of fatigue life. Journal of Sound and Vibration 76, 281–308.

Buhler, W., Frendi, A., 2004. Effect of fluid-wall shear stress on nonlinear beam vibration. Journal of Sound and Vibration 270, 793–811.

Chung, T.J., 1996. Applied Continuum mechanics. Cambridge University Press, New York.

Frendi, A., 1997a. Coupling between a supersonic turbulent boundary layer and a flexible structure. AIAA Journal 35, 58–66.

Frendi, A., 1997b. Effect of pressure gradients on plate response and radiation in a supersonic turbulent boundary layer. NASA-CR-201691.

Frendi, A., 2001. Effect of wall shear stress on structural vibration. AIAA Journal 39, 737–740.

Frendi, A., Robinson, J., 1993. Effect of acoustic coupling on random and harmonic plate vibrations. AIAA Journal 31, 1992–1997.

Frendi, A., Maestrello, L., Bayliss, A., 1994. Coupling between plate vibration and acoustic radiation. Journal of Sound and Vibration 177, 207–226.

Hoff, C., Pahl, P.J., 1988a. Development of an implicit method with numerical dissipation from a generalized single-step algorithm for structural dynamics. Computer Methods in Applied Mechanics and Engineering 67, 367–385.

Hoff, C., Pahl, P.J., 1988b. Practical performance of the θ_1-method and comparison with other dissipative algorithms in structural dynamics. Computer Methods in Applied Mechanics and Engineering 67, 87–110.

Maestrello, L., 1969. Radiation from and panel response to a supersonic turbulent boundary layer. Journal of Sound and Vibration 10, 262–295.

Maestrello, L., Frendi, A., 1992. Nonlinear vibration and radiation from a panel with transition to chaos. AIAA Journal 30, 2632–2638.

Mei, C., Prasad, C.B., 1987. Effects of nonlinear damping on random response of beams to acoustic loading. Journal of Sound and Vibration 117, 173–186.

Reinhall, P.G., Miles, R.N., 1989. Effects of damping and stiffness on the random vibration of non-linear periodic plates. Journal of Sound and Vibration 131, 33–42.

Robinson, J., Mei, C., 1989. The influence of nonlinear damping on the random response of panels by time domain simulation. AIAA Paper 89-1104.

Robinson, J., Rizzi, S., Clevenson, S., Daniels, E., 1992. Large deflection random response of flat and blade stiffened carbon–carbon panels. AIAA-92-2390.

Vinson, J.R., 1974. Structural Mechanics: The Behavior of Plates and Shells. Wiley, New York.